ACS OMEGA

http://pubs.acs.org/journal/acsodf

Article

In Situ Spectroscopic Studies of NH_3 Oxidation of Fe-Oxide/Al_2O_3

Byeong Jun Cha, Ji Yoon Choi, Soo Hyun Kim, Shufang Zhao, Sher Ali Khan, Beomgyun Jeong, and Young Dok Kim*

Cite This: *ACS Omega* 2023, 8, 18064−18073

Read Online

ACCESS | Metrics & More | Article Recommendations | Supporting Information

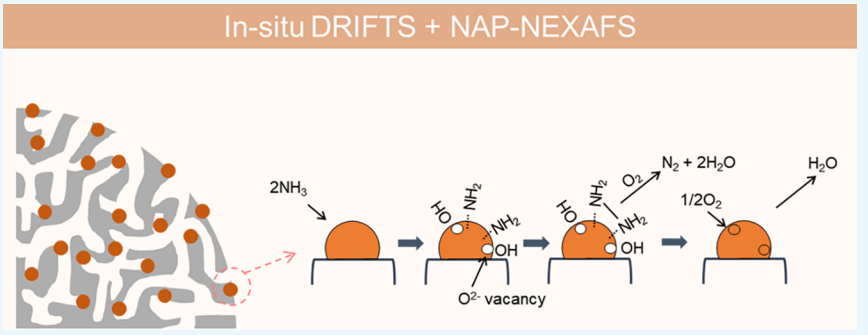

ABSTRACT: Simple temperature-regulated chemical vapor deposition was used to disperse iron oxide nanoparticles on porous Al_2O_3 to create an Fe-oxide/Al_2O_3 structure for catalytic NH_3 oxidation. The Fe-oxide/Al_2O_3 achieved nearly 100% removal of NH_3, with N_2 as a major reaction product at temperatures above 400 °C and negligible NO_x emissions at all experimental temperatures. The results of a combination of in situ diffuse reflectance infrared Fourier-transform spectroscopy and near-ambient pressure−near-edge X-ray absorption fine structure spectroscopy suggest a N_2H_4-mediated oxidation mechanism of NH_3 to N_2 via the Mars−van Krevelen pathway on the Fe-oxide/Al_2O_3 surface. As a catalytic adsorbent—an energy-efficient approach to reducing NH_3 levels in living environments via adsorption and thermal treatment of NH_3—no harmful NO_x emissions were produced during the thermal treatment of the NH_3-adsorbed Fe-oxide/Al_2O_3 surface, while NH_3 molecularly desorbed from the surface. A system with dual catalytic filters of Fe-oxide/Al_2O_3 was designed to fully oxidize this desorbed NH_3 to N_2 in a clean and energy-efficient manner.

1. INTRODUCTION

Ammonia (NH_3) is an indispensable substance in the modern industry, as it is not only essential for the production of fertilizers, plastics, and useful chemicals but also useful in purifying waste water or storing hydrogen for fuel applications.[1−5] However, because NH_3 is caustic and hazardous, NH_3 can cause serious health and environmental problems when released to the atmosphere.[6] In addition, noxious odors caused by NH_3 in living environments, particularly near agricultural areas, have become a major social issue.[7−9]

To reduce NH_3 emissions, various strategies such as scrubbing, condensation, biofiltration, thermal oxidation, adsorption, and catalytic oxidation can be applied at the NH_3 emission sources.[10−16] Catalytic oxidation is a promising technique for field applications; ideally, catalytic filters for NH_3 oxidation can work permanently without the need for exchanges or regeneration. A representative example is selective catalytic oxidation of NH_3, in which NH_3 is used to reduce nitrogen oxide (NO_x) generated by fossil-fuel combustion in power plants or diesel vehicles, and its slip to the atmosphere can be reduced by this selective catalytic oxidation technology, which normally operates under an NH_3/NO_x ratio of approximately 0.9−0.95 and a high O_2 concentration.[2,17,18] Nanoparticles of platinum-group metals or earth-abundant transition metals such as Ti, Fe, Mn, V, and Cu can be used for this application at 250−500 °C.[2,16,19] Platinum-group metals have a high NH_3 conversion rate at low temperature in general, but significant NO_x emission is a major limitation for their application. Nanostructures of Ti, Mn, V, and Cu oxides can show high NH_3 conversion at low temperature with low NO_x emission, but their low thermal stability has been considered as a limitation. The operating temperature of these catalysts can be reached easily when fossil-fuel combustion is taking place nearby, and little external thermal energy is therefore required to increase catalyst temperature.

However, to remove NH_3 from a living environment, catalytic technology with improved energy efficiency and reactivity in the absence of NO_x is needed. In many living

Received: March 1, 2023
Accepted: April 7, 2023
Published: May 11, 2023

environments, external energy should be applied to increase the catalyst temperature, and it is not energy-efficient to maintain catalytic operating temperatures, particularly when NH_3 is not continuously emitted or is at low concentrations. Incorporation of catalytic nanoparticles into porous adsorbent materials with a high surface area is an effective option that can take advantages of both catalysts and adsorbents, reducing energy costs.[20−22] At room temperature (RT), NH_3 can be adsorbed on the surface of these materials, and during the intermittent thermal oxidation process to regenerate the adsorption sites, adsorbed NH_3 can be converted into nonharmful N_2 with the help of catalytic particles. It is important to minimize the molecular desorption of NH_3 and emissions of harmful NO_x gases during this process.

In the present work, simple temperature-regulated chemical vapor deposition (tr-CVD) was used to deposit catalytically active iron oxide (Fe-oxide) nanoparticles on mesoporous alumina (Al_2O_3) beads in a highly dispersed manner,[23−25] and this structure was used for NH_3 removal. The Al_2O_3-supported Fe-oxide nanoparticles (Fe-oxide/Al_2O_3) were able to oxidize NH_3 to N_2 through a hydrazine (N_2H_4)-mediated pathway with no harmful gas emission including NH_3 and NO_x at temperatures above 400 °C. When Fe-oxide/Al_2O_3 was used as catalytic adsorbent, molecular desorption of NH_3 occurred during the thermal treatment of NH_3-covered surfaces. To eliminate NH_3 emissions at a minimal energy cost, a system with two interconnected catalytic filters was designed. By heating the rear side of the catalytic filter prior to the thermal treatment of the front-side filter, emissions of NH_3 to the atmosphere were fully prevented.

From the fundamental point of view, the present study provides novel information on the mechanism responsible for NH_3 oxidation of an Fe-oxide catalyst. Previous studies determined N_2 selectivity indirectly by measuring the removed NH_3 that was not converted into NO_x,[17,26,27] whereas in the present work, the amount of generated N_2 was measured directly, which enabled consideration of reaction intermediates on the surface during the reaction. In addition, the present work combined in situ diffuse reflectance infrared Fourier-transform spectroscopy (DRIFTS) with near-ambient pressure−near-edge X-ray absorption fine structure spectroscopy (NAP-NEXAFS), which allowed us to elucidate both structural changes in reactants during the catalytic reaction and the catalyst itself. Using this combination, N_2H_4-mediated oxidation of NH_3 to N_2 via the Mars−van Krevelen pathway could be suggested. This study shows that NAP-NEXAFS can not only be applied to studies of model catalyst structures but also used for unveiling practical catalyst structures under operating conditions. From an application point of view, the system of dual catalytic filters designed in the present study can solve problems that arise when catalytic adsorbent materials are used to remove NH_3, specifically the re-emission of NH_3 during thermal treatment of NH_3-covered surfaces.

2. MATERIALS AND METHODS

2.1. Catalyst Preparation. Fe-oxide nanoparticles were deposited on Al_2O_3 using temperature-regulated chemical vapor deposition (tr-CVD).[23−25,28] The tr-CVD is a simple one-pot approach to incorporate small metal oxide nanoparticles into a porous substrate via diffusion of metal precursor throughout the porous network and its subsequent oxidation to metal oxide species. This method can be more environmentally friendly than liquid phase methods because it does not require any organic solvent. In addition, this method can take advantage of using vapor, which enables efficient incorporation of small nanoparticles into not only on the external surface of the substrate but also into its small internal meso- or micropores. This technique can be applied to various other substrates including SiO_2, zeolite, and TiO_2.[22,29,30]

Inside the tr-CVD chamber, the Fe precursor ferrocene, $Fe(Cp)_2$, (Aldrich) and Al_2O_3 beads (bead size: 1 mm; mean pore size: 11.6 nm, Sasol) were placed separately. In the first step, the Fe precursors evaporated and diffused into the entire porous network of Al_2O_3 at 60 °C over 2 h. In the second step, the diffused ferrocene molecules oxidized into Fe-oxide nanoparticles at 200 °C for 12 h. In the present work, 2.5 g of ferrocene and 10 g of Al_2O_3 beads were used to prepare the Al_2O_3-supported Fe-oxide nanoparticles. This structure was then annealed at 750 °C for 2 h in dry air (30 mL/min), and the prepared sample was labeled Fe-oxide/Al_2O_3. Details of the tr-CVD are provided in the Supporting Information (Figure S1).

2.2. Characterization. The loading of Fe on Al_2O_3 was measured using inductively coupled plasma-optical emission spectroscopy (ICP-OES, PerkinElmer AVIO 550Max, Varian). Dispersion of Fe-oxide on a mesoporous network of Al_2O_3 was confirmed by energy dispersive spectroscopy and scanning electron microscopy (SEM, JEOL, JSM-7100F). The Fe-oxide/Al_2O_3 beads were cut in half, and cross-sections were used for this analysis. The geometrical structure of the Fe-oxide particles was analyzed by high-angle annular dark field (HAADF) scanning transmission electron microscopy (STEM, JEOL, JEM ARM 200F). The surface area and pore size of the Fe-oxide/Al_2O_3 were estimated using the Brunauer−Emmett−Teller (BET) and Barret−Joyner−Halenda (BJH) methods, respectively, based on N_2 adsorption isotherm analysis (3Flex, Micromerities). The chemical structure of Fe-oxide on Al_2O_3 was analyzed by X-ray photoelectron spectroscopy (XPS). Mg K-alpha radiation (1253.6 eV) was used as an X-ray source, and the kinetic energy of the photoelectrons was measured with a concentric hemispherical analyzer (PHOIBOS 150 1D-DLD, SPECS, Germany).

2.3. Catalytic Activity Test: Experimental Setup and Procedures. The catalytic activity of Fe-oxide/Al_2O_3 for NH_3 oxidation was evaluated using a flow-type reactor connected to an online gas chromatograph (GC, Hewlett Packard, HP 6890). The GC was equipped with two capillary columns, each of which was connected to a thermal conductivity detector with a detection limit of approximately 400 ppm. A CP-Volamine column (Agilent Technologies, 30 m × 32 μm) was used to separate NH_3, H_2O, and nitrous oxide (N_2O) from the gas mixture, while a CP-Molseive 5A column (Agilent Technologies, 25 m × 30 μm) was used for N_2, nitric oxide (NO), and nitrogen dioxide (NO_2).

To measure activity with respect to reactor temperature, 4.0 g of Fe-oxide/Al_2O_3 (or bare Al_2O_3) was first heated to 750 °C for 2 h in dry air. The temperature was decreased to 450 °C, and from this point, the temperature was decreased to 200 °C at −1 °C/min. Simultaneously, a He-balanced gas mixture containing 2% NH_3 and 6% O_2 (total 50 mL/min) was introduced into to the reactor. The gas from the reactor outlet was analyzed by the GC periodically during this process. The catalytic stability of Fe-oxide/Al_2O_3 (or bare Al_2O_3) at 450 °C was also tested under the same catalyst-annealing and gas-flow conditions. These measurements were also taken under 30 and 60% of relative humidity (RH) conditions.

https://doi.org/10.1021/acsomega.3c01380
ACS Omega 2023, 8, 18064−18073

For the adsorption and thermal treatment experiment of NH_3, 50 mL/min gas mixture containing 2% NH_3 and 6% O_2 balanced with He was introduced into the reactor along with 4 g of the catalyst at RT for NH_3 adsorption. After the concentration of NH_3 at the reactor outlet reached 2%, indicating adsorption saturation, the flow of NH_3 was stopped while maintaining O_2 and He flow until the weakly adsorbed NH_3 or gaseous NH_3 in the reactor was completely purged out. When NH_3 was no longer detected by the GC, a temperature-programmed oxidation experiment was performed by increasing the reactor temperature from RT to 500 °C at a ramping rate of +1 °C/min under the same gas-flow condition as used in the purging stage. The concentration of the desorbed species from the catalyst surface was analyzed with respect to temperature. This adsorption and thermal treatment process was repeated four times without replacing the catalyst.

Adsorption and thermal oxidation of NH_3 using a system of dual catalytic filters was allowed to proceed in the following order (Figure 5 provides a schematic of the system): first, 2 g of Fe-oxide/Al_2O_3 was placed in each reactor (reactor 1 and reactor 2), after which 50 mL/min He-balanced gas mixture containing 2% NH_3 and 6% O_2 was injected into reactor 1 at RT. At this time, the gas mixture passing through reactor 1 was directed to the online GC without passing to reactor 2. Second, once the catalyst in reactor 1 was saturated with NH_3, the NH_3 flow was stopped while maintaining the flow of He and O_2, and the temperature of reactor 2 was rapidly increased to 400 °C. Third, when the temperature of reactor 2 reached 400 °C, the temperature of reactor 1 was increased from RT to 400 °C at a ramping rate of +1 °C/min to desorb or oxidize the NH_3 adsorbed on the Fe-oxide/Al_2O_3 in reactor 1. In this step, the gas mixture that passed through reactor 1 was directed to reactor 2 before the online GC. Fourth, with the increasing temperature of reactor 1, the concentration of N_2 or NH_3 was analyzed by the online GC. Finally, steps 1 through 4 were repeated without replacing the catalyst. Further details of experimental setup and their procedures are provided in the Supporting Information (Figure S2).

2.4. In Situ DRIFTS and NAP-NEXAFS. Catalytic oxidation mechanism of NH_3 on Fe-oxide/Al_2O_3 surfaces was studied using in situ DRIFTS and NAP-NEXAFS spectroscopy. For DRIFTS, a Fourier-transform infrared (FT-IR) spectrometer (Thermo Fisher Scientific, Nicolet iS10, USA) combined with a praying mantis DRIFTS accessory (Harrick Scientific, USA) was used. In 10 mg of mechanically ground Fe-oxide/Al_2O_3 diluted with 190 mg KBr, 50 mL/min He-balanced gas mixture containing 2% NH_3 and 6% O_2 was flowed, and FT-IR spectra were obtained at 30, 250, 350, and 450 °C. The spectrum of each temperature was obtained using a fresh catalyst sample. The infrared spectrum in the presence of bare Al_2O_3 at 450 °C was obtained for comparison.

NAP-NEXAFS analysis on Fe-oxide/Al_2O_3 was carried out in the 8A2 AP-XPS beam line constructed at the Pohang Accelerator Laboratory (PAL). A 1.2 mg sample of ground Fe-oxide/Al_2O_3 powder in ethanol was drop-casted onto a 1 × 1 cm^2 silicon wafer for analysis. Using a back-filling method and laser heating, atmospheric conditions and the sample temperature were controlled. Fe L edge spectra at 450 °C or ultrahigh vacuum (UHV) conditions at RT were obtained using the total electron yield mode. Residual gas analysis was conducted in parallel to determine whether the reaction atmosphere was maintained during surface analysis. The obtained Fe L edge spectra were deconvoluted using mixed functions of Gaussian and Lorentzian. For each component, peak width was fixed while its position was adjusted within 0.1 eV (Figure S7 and Table S1).

3. RESULTS AND DISCUSSION

3.1. Characterizations. The tr-CVD-prepared Fe-oxide/Al_2O_3 beads, with an Fe content of 5.39 wt % as determined by ICP-OES analysis (Table 1), exhibited a yellowish color due to the incorporated Fe-oxide on Al_2O_3 (Figure 1a). In an elemental Fe mapping image of the cross-sectional plane of an Fe-oxide/Al_2O_3 bead (Figure 1b), the Fe is distributed evenly throughout the entire bead of Al_2O_3 with porous networks. In XRD analysis of Fe-oxide/Al_2O_3, diffraction peaks related to Fe-oxide were not visible, which also implies high dispersion of Fe-oxide on Al_2O_3 (Figure S3). Inspecting the structure of the Fe-oxide more closely with HAADF STEM imagery (Figure 1c), round protrusions were observed, the mean size of which was estimated to be ∼1 nm (see particle size distribution plot in the inset of Figure 1c). The protrusions were identified as the particles of Fe compounds from the line EDS analysis (Figure 1d).

Table 1. Fe Content, BJH Pore Size, and BET Surface Area of Al_2O_3 and Fe-Oxide/Al_2O_3

	Al_2O_3	Fe-oxide/Al_2O_3
Fe content (wt %)		5.39
BJH average pore size (nm)	12.2	12.1
BET surface area (m^2/g)	160.9	139.2

The pore structure of Al_2O_3 was not significantly altered upon deposition of Fe-oxide nanoparticles, based on N_2-adsorption and desorption isotherm analysis. Both Al_2O_3 and Fe-oxide/Al_2O_3 showed typical isotherm plots of mesoporous materials (Figure 1e).[22,31] Mono- and multilayer adsorption of N_2 takes place at low pressures, while at high pressures, capillary condensation and evaporation take place in mesopores, indicated by the hysteresis loop in the plot. Only a slight decrease in the quantity adsorbed was found upon the deposition of Fe-oxide, which is related to the decrease of BET surface area of Al_2O_3 from 160.9 to 139.2 m^2/g after the Fe-oxide deposition (Table 1). There was no notable change in the pore-size distribution plot (inset, Figure 1e) upon Fe-oxide deposition except for a slight decrease in total pore volume. Accordingly, the average pore size estimated by the BJH method (approximately 12 nm) remained almost constant after Fe-oxide deposition on Al_2O_3 (Table 1). The decrease in pore volume upon Fe-oxide deposition was likely due to the demolition of some Al_2O_3 pores upon annealing in the presence of Fe-oxide due to the strong interaction between Al_2O_3 and Fe-oxide, rather than due to the blocking effect of mesopores by Fe-oxide nanoparticles, which are much smaller than the average pore size of Al_2O_3.[23,25]

The chemical structure of the Al_2O_3-supported Fe-oxide nanoparticles was studied using XPS. In Figure 1f, the Fe $2p_{3/2}$ spectrum is shown with a peak deconvolution based on the Gupta and Sen (GS) method, which considers various possible factors related to the peak broadening of Fe 2p (e.g., electrostatic interactions, L-S coupling between unpaired 3d electrons in a photoionized Fe cation and its 2p hole, and crystal field interactions).[32,33] Using the GS method, six independent components—prepeak, surface peak, and multiple

https://doi.org/10.1021/acsomega.3c01380
ACS Omega 2023, 8, 18064−18073

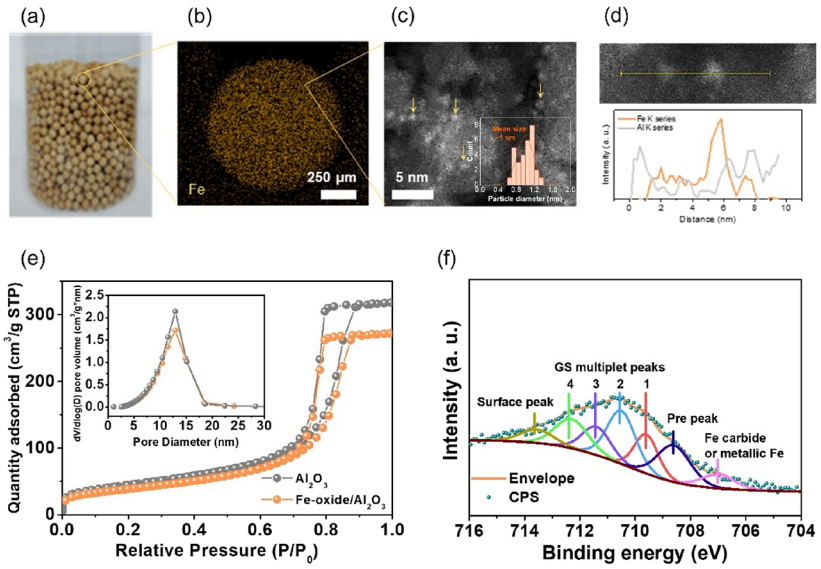

Figure 1. (a) Picture of Fe-oxide/Al_2O_3 beads. (b) Fe elemental mapping image of the cross-sectional plane of a Fe-oxide/Al_2O_3 bead. (c) HAADF-STEM image of Fe-oxide/Al_2O_3, and (d) line EDS mapping analysis result of white protrusions observed in the STEM image. Inset of (c): particle size distribution of the protrusions. (e) N_2 adsorption and desorption isotherm plots of bare Al_2O_3 and Fe-oxide/Al_2O_3. Inset: pore size distribution plots based on the isotherm analysis. (f) Fe $2p_{3/2}$ XPS spectrum obtained from Fe-oxide/Al_2O_3 with peak deconvolution based on the Gupta and Sen method.

peaks 1 to 4 ranging from 708.5 to 713.8 eV—were required to fit an Fe $2p_{3/2}$ spectrum of a single phase of Fe-oxide, and each phase of Fe-oxide had unique ratios among peaks 1−4.[34] In our Fe-oxide/Al_2O_3, ratios among peaks 1−4 were 22, 35.89, 19.14, and 22.97%, respectively, which did not perfectly match any of single phase of Fe-oxide, implying that our Fe-oxide nanoparticles were instead a mixture of various Fe-oxide phases (e.g., FeO, Fe_2O_3, Fe_3O_4, FeOOH, ...).[20,23,25] Raman spectroscopy analysis of the Fe-oxide/Al_2O_3 could also indicate the coexistence of various phases of Fe-oxide (Figure S4). Although the additional small component at 707 eV can be attributed to either Fe carbide or metallic Fe, its relative composition was less than 10%. In addition, in the X-ray absorption spectroscopic analysis (Figure 3b), which generally has higher informative depth than XPS, these components are not clearly visible, indicating that they contributed only marginally to overall the composition, and the majority of the Fe in our catalyst sample was in oxidized forms.

3.2. Impact of Reaction Temperature and Humidity on Catalytic NH_3 Oxidation of Fe-Oxide/Al_2O_3. NH_3 removal and N_2 selectivity with respect to temperature under dry and humid (30% and 60% RH) conditions obtained from Fe-oxide/Al_2O_3 are displayed in Figure 2. The parameters obtained from bare Al_2O_3 at 450 °C under dry conditions are also included for comparison. Under dry conditions, 90% or greater NH_3 removal was observed above 400 °C, after which it decreased gradually with temperature, reaching approximately 10% from 250 °C. N_2 selectivity under dry conditions also decreased with reactor temperature. Nitrogen oxide gases (NO, NO_2, or N_2O) were not detected over the entire temperature range under our experimental conditions. That is, the majority of the removed NH_3 that was not converted to gas phase N_2 could reside on the surface of Fe-oxide/Al_2O_3 in reaction intermediate states or adsorbed forms. When bare Al_2O_3 was used, NH_3 removal and N_2 selectivity at 450 °C were approximately 29 and 58%, respectively, which are much lower than those from Fe-oxide/Al_2O_3. The results show that

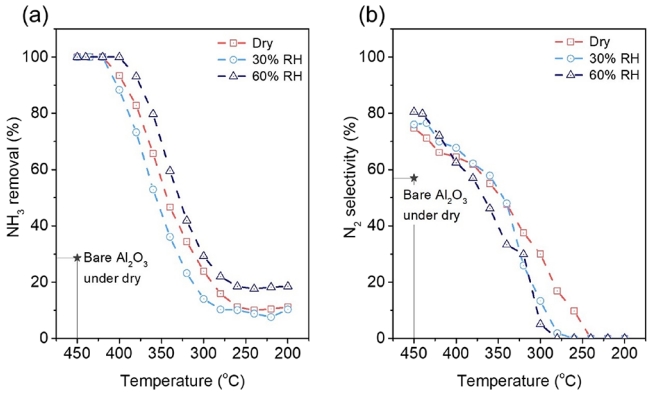

Figure 2. (a) NH_3 removal and (b) N_2 selectivity with respect to temperature under dry, 30%, and 60% RH conditions obtained from Fe-oxide/Al_2O_3. The parameters obtained from bare Al_2O_3 at 450 °C under dry conditions are also included for comparison. Reaction conditions: 4 g catalyst in a fixed bed, 50 mL/min He balanced gas mixture containing 2% NH_3, and 6% O_2.

Fe-oxide deposition on Al_2O_3 can enhance not only the removal of NH_3 but its selectivity to N_2 as well.

In comparison with dry conditions, NH_3 removal under a 30% humid condition was similar at temperatures above 420 °C, but it became slightly lower below this temperature. N_2 selectivity was affected only marginally by humidity at temperatures above 350 °C, but below this temperature, the presence of humidity reduced N_2 selectivity. When humidity increased from 30 to 60%, NH_3 removal did not decrease further but actually increased in a broad range of temperature, while N_2 selectivity seemed to decrease slightly in the range of 320−400 °C. It can be speculated that H_2O molecules can compete with NH_3 molecules for adsorption sites, while they can also help conversion of NH_3 to surface residual nitrogen compounds.[35,36] The former role of H_2O can induce reduction of NH_3 removal; however, from a certain level of humidity, the

https://doi.org/10.1021/acsomega.3c01380
ACS Omega 2023, 8, 18064−18073

later pathway can become more activated, leading to the improved NH_3 removal and the reduced N_2 selectivity.

Based the observations shown in Figure 2, Fe-oxide/Al_2O_3 can effectively oxidize NH_3 with high N_2 selectivity and negligible nitrogen oxide gas emissions at temperatures above approximately 400 °C. The high catalytic activity and selectivity to N_2 could also be maintained for at least 7 h under both dry and humid conditions at 450 °C (Figure S5).

3.3. Surface Reaction Mechanism of NH_3 Oxidation on Fe-Oxide/Al_2O_3. *3.3.1. In Situ DRIFTS.* In situ DRIFTS analysis was used to reveal the NH_3 oxidation mechanism of Fe-oxide/Al_2O_3. Figure 3a shows infrared spectra obtained

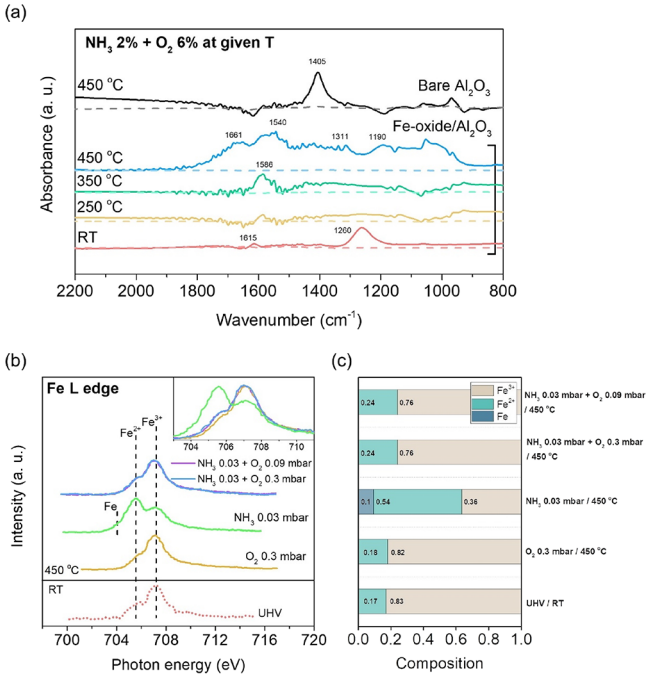

Figure 3. (a) In situ DRIFTS spectra obtained from Fe-oxide/Al_2O_3 at RT, 250, 350, and 450 °C under NH_3 oxidation conditions. Each spectrum was obtained after 60 min of reactant gas flow to a fresh sample in each condition. Reaction conditions: 10 mg of mechanically ground sample diluted with 190 mg KBr, 50 mL/min He balanced gas mixture containing 2% NH_3 and 6% O_2. (b) Fe L edge NAP-NEXAFS spectra obtained from Fe-oxide/Al_2O_3 under UHV at RT, and under various atmospheric conditions at 450 °C. (c) Comparison of Fe state composition estimated from the peak deconvolution of Fe L edge spectra.

from Fe-oxide/Al_2O_3 at RT and 250, 350, and 450 °C under the same atmospheric conditions as those in the activity test (2% NH_3 and 6% O_2, He-balanced, 50 mL/min). An infrared spectrum obtained from bare Al_2O_3 at 450 °C under the same atmospheric condition is also displayed. Each spectrum in Figure 3a was obtained after 60 min of reactant gas flow to a fresh sample at each temperature until the spectral shape no longer changed significantly with time. The infrared spectrum obtained before flowing the reactant gas was used for a background in each temperature, and each dotted line represents the spectrum obtained immediately after reactant gas flow. Spectral changes with reactant gas flow time in each reaction condition are provided in Figure S6. The IR signal assignments of the features observed in DRIFTS analysis are summarized in Table 2.

Table 2. IR Signal Assignments of the Features Observed in DRIFTS Analysis

peak or band position (cm^{-1})	assignment	ref
1260 (strong), 1615	symmetric and asymmetric N−H bending modes of physisorbed NH_3	27,37−39
1586	N−H scissoring mode of $-NH_2$	37,38
1190	N−N stretching mode of adsorbed N_2H_4	40,42
1311	NH_2 wagging mode of adsorbed N_2H_4	40,42
1540	NH_2 scissoring mode of adsorbed N_2H_4	40,42
1661	symmetric N−H bending mode of NH_4^+	40
1405	N−O stretching mode of NO_3^-	38,40,41

At RT, the two infrared absorption peaks at 1260 and 1615 cm^{-1} can be attributed to symmetric and asymmetric N−H bending modes of physiosorbed NH_3, respectively.[27,37−39] Most of the NH_3 molecules appeared to adsorb on Fe-oxide/Al_2O_3 surfaces, maintaining their structure at RT. With the increase in reaction temperature to 250 °C, noticeable changes in spectral shapes were observed; a broad signal appeared between 1100 and 1500 cm^{-1}, and a more distinct peak could be seen at 1586 cm^{-1}. Due to the broadness of the infrared signal, it is difficult to interpret the origin of the absorbance increase at 1100−1500 cm^{-1}. However, given that the peak at 1586 cm^{-1} is typical of N−H scissoring of amino $-NH_2$) groups[37,38] and that other various bending modes of N−H from $-NH_2$ generally fall into the 1100−1500 cm^{-1} range,[37,38] it is likely that NH_3 dissociatively adsorbs as $-NH_2$ on an Fe-oxide/Al_2O_3 surface at 250 °C. An imine group (=N−H) can also exist from the dissociative adsorption of NH_3 on the catalyst surface, as its bending modes generally appear at 1100−1500 cm^{-1}.[37,40]

It is important to note that formation of nitrogen oxide compounds (NO, NO_2, or N_2O) did not likely form at 250 °C, not only because they were not detected as gaseous forms (Figure 2), but also because their related signals were not clearly resolved in the infrared spectrum. For example, in most cases that use Fe-oxide catalysts, a nitroxyl group (−HNO) is formed as a reaction intermediate in the formation of the nitrogen oxide compounds.[38,40] It generally shows distinctive peaks of N−O stretching near 1480 and 1529 cm^{-1}, and these were not clearly observed in our case. In addition, adsorbed NO or NO_2 typically produce an infrared peak of N−O stretching at 1800−1900 cm^{-1},[37] while adsorbed N_2O shows an infrared peak from N−N stretching at 2100−2200 cm^{-1}, and these were also not clearly observed in our experiments. Formation of nitrate (NO_3^-) is possible but less likely, as its N−O stretching vibration generally shows a sharp peak at 1300−1400 cm^{-1}.[38,40,41] The wiggling fine structures with fixed interval in 1400−1800 cm^{-1} are attributed to the rotational modes of water vapor, probably formed by the NH_3 oxidation reaction.

When increasing the temperature to 350 °C, the infrared signals at 250 °C increased in intensity, with no other prominent qualitative change, and at 450 °C, clear information on the NH_3 oxidation mechanism was obtained; in addition to the absorbance increase at 1100−1500 and 1586 cm^{-1}, new features were observed at 1190, 1311, 1540, and 1661 cm^{-1}. The former three features at 1190, 1311, and 1540 cm^{-1} are most likely attributable to N−N stretching, NH_2 wagging, and NH_2 scissoring modes of adsorbed hydrazine (N_2H_4), respectively.[40,42] The appearance of these features implies that $-NH_2$ species generated from the dissociative adsorption

https://doi.org/10.1021/acsomega.3c01380
ACS Omega 2023, 8, 18064−18073

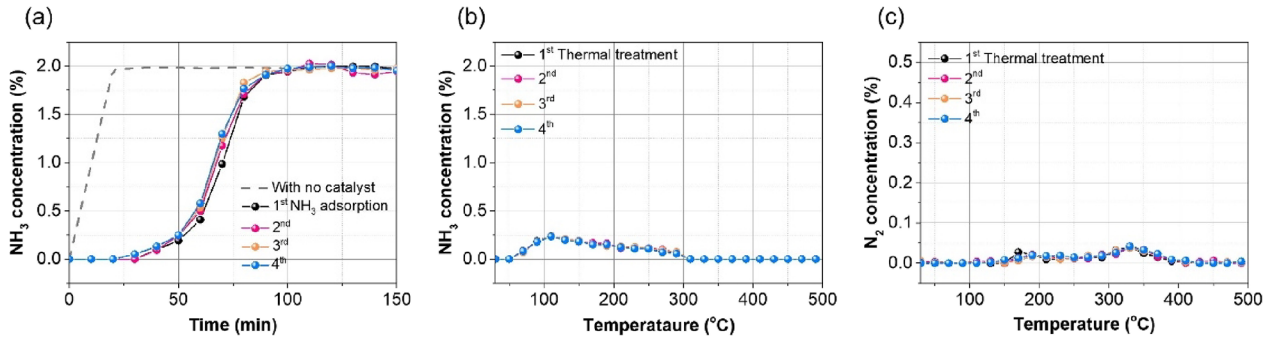

Figure 4. (a) Change of NH_3 concentration measured at the reactor outlet as a function of NH_3 flow time at RT in the presence of Fe-oxide/Al_2O_3. The gray line represents the change of NH_3 concentration without the catalyst. Change of (b) NH_3 and (c) N_2 concentration with respect to the temperature in the thermal treatment process after the NH_3 adsorption at RT. The adsorption and thermal treatment was repeated four times without replacing the catalyst, and the result of each cycle is included in the figures. Reaction conditions: 4 g of catalyst in a fixed bed, 50 mL/min He balanced gas mixture containing 2% NH_3 and 6% O_2 for NH_3 adsorption, and 49 mL/min 6% O_2 balanced with He for the thermal treatment.

of NH_3 can form N−N bonds and dimerize into N_2H_4 on an Fe-oxide/Al_2O_3 surface, which is a key intermediate for the oxidation of NH_3 to N_2 in many transition metal oxide catalysts.[2,42−44] From comparing IR spectra of as-prepared and hydrazine-adsorbed Fe-oxide/Al_2O_3, the N_2H_4 formation during the NH_3 oxidation at high temperature could be also supported (Figure S8). The band appearing at 1661 cm^{-1} can be most likely assigned to the symmetric N−H bending mode of ammonium ions (NH_4^+), formation of which can be also supported by the concomitant absorbance increase near 1450 cm^{-1} attributed to its asymmetric N-H bending.[40] Formation of NH_4^+ can be also involved in N_2H_4 formation; at high temperatures, NH_3 can strongly adsorb on the surface, forming NH_4^+, and NH_4^+ reacts with active oxygen species to form $-NH_2$ and H_2O, after which $-NH_2$ can be converted to N_2H_4.[45] From the DRIFTS analysis, we speculated that $-NH_2$ species can be actively formed at low temperatures by dissociative NH_3 adsorption on the catalyst, but the formation of N−N bonds between two $-NH_2$ species can be facilitated at high temperatures, which could increase N_2 selectivity. The dissociatively adsorbed NH_3, NH_4^+, and N_2H_4 structures on the surface of Fe-oxide/Al_2O_3 at elevated temperature can account for the missing portion of N_2 selectivity, since the only gas product we could detect at a significant level during the NH_3 oxidation was N_2.

For bare Al_2O_3 without Fe-oxide, a prominent peak at 1405 cm^{-1} attributable to NO_3^- was evident at 450 °C without indication of N_2H_4 formation. From activity measurements (Figure 2), bare Al_2O_3 could convert NH_3 to N_2 with 58% of N_2 selectivity at 450 °C under dry conditions. Based on these results, bare Al_2O_3 seems to catalyze oxidation of NH_3 to N_2 in a different mechanism from Fe-oxide/Al_2O_3. An internal SCR mechanism where NO is formed by NH_3 oxidation, which then react with other NH_3 to produce N_2, or −HNO intermediated mechanism is possible.[2] Both of these pathways can induce surface poisoning by accumulation of nitrogen oxide species like NO_3^-, which can reduce N_2 selectivity. The DRIFTS results overall suggest that Fe-oxide nanoparticles suppress the formation of NO_3^- from NH_3 and simultaneously facilitate conversion of NH_3 to N_2 via the N_2H_4-mediated pathway.

3.3.2. NAP-NEXAFS. While in situ DRIFTS analysis was used to study how the structure of reactant molecules changes on the surface during the reaction, NAP-NEXAFS analysis was employed to investigate which change the structure of catalyst itself undergoes during the reaction. Figure 3b shows the Fe L edge spectra from Fe-oxide/Al_2O_3 under UHV conditions at RT or various atmospheric conditions at 450 °C. The Fe Ledge spectrum under UHV at RT has two main features at 705.8 and 707.6 eV that are attributable to Fe's oxidation states of 2+ and 3+, respectively.[46,47]

In an O_2 atmosphere (0.3 mbar) at 450 °C, the ratio of Fe^{2+} to Fe^{3+} was similar to that in UHV conditions at RT. In an NH_3 atmosphere (0.03 mbar), the ratio of Fe^{2+} to Fe^{3+} increased dramatically, along with the appearance of a shoulder at approximately 705 eV attributable to metallic Fe. Lattice oxygen atoms of Fe-oxide were consumed by their reaction with NH_3 at the surface, contributing to a lower Fe^{3+} ratio. When O_2 was added here, Fe^{3+} became dominant again, producing a spectral shape that at first glance appears to be similar to that in the O_2-only condition. However, when superimposed with the spectrum under O_2 only, it is clear that the ratio of Fe^{2+} to Fe^{3+} was higher in the presence of NH_3 (inset of Figure 3b), indicating that some lattice oxygens of Fe-oxide are being reduced by NH_3 oxidation. From Figure 3c, showing the composition of the Fe state estimated from the peak deconvolution of Fe L edge spectra in Figure 3b, the increase of Fe^{2+} composition upon adding NH_3 to the O_2 atmosphere could be more clearly seen. These results suggest that an Fe-oxide surface does not simply provide adsorption sites for NH_3 and O_2 without structural change but plays a more active role, based on a Mars−van Krevelen mechanism;[48−50] lattice oxygen of Fe-oxide is used for the oxidation of adsorbed NH_3 to $-NH_2$, resulting in the reduction of Fe-oxide and the formation of product molecules such as H_2O, which later desorb from the surface. The concomitantly generated oxygen-vacancy sites are replenished by dissociative adsorption of gaseous O_2. Combining the DRIFTS and NAP-NEXAFS results, dissociative adsorption of NH_3 forming $-NH_2$ species took place, the Fe-oxide deposited on Al_2O_3 could facilitate this oxidation process of NH_3 to $-NH_2$ by its partial reduction, and the generated surface $-NH_2$ species could further dimerize to form N_2H_4 species, desorbing as N_2 gas.

3.4. NH_3 Adsorption and Thermal Treatment of NH_3−Covered Fe-Oxide/Al_2O_3. For environments where NH_3 flows noncontinuously or its concentration is low, it is not necessary to maintain high catalyst operating temperatures to decompose NH_3, and using a catalytic adsorbent can be a superior strategy with an improved energy efficiency. NH_3 can be adsorbed onto a catalytic adsorbent material at RT, and

https://doi.org/10.1021/acsomega.3c01380
ACS Omega 2023, 8, 18064−18073

when all adsorption sites are saturated, adsorbed NH_3 can be thermally oxidized into less- or nonharmful gases; in this way, thermal energy consumption for NH_3 decomposition could be reduced. We repeated a cycle of NH_3 adsorption at RT and subsequent heating to 500 °C four times consecutively without changing the catalyst.

Figure 4a depicts the change in NH_3 concentration at the reactor outlet as a function of NH_3 flow time at RT in the presence of Fe-oxide/Al_2O_3 in each cycle. The gray line, which represents the change in NH_3 concentration without the catalyst, shows that NH_3 concentrations reached 2% within 20 min. However, it took much longer (approximately 100 min) to reach 2% in the presence of the catalyst due to NH_3 adsorption on the Fe-oxide/Al_2O_3. This breakthrough curve was almost identical in all four cycles, indicating that the adsorption capacity of Fe-oxide/Al_2O_3 recovered through heating without significant deactivation.

Figure 4b,c shows changes of NH_3 and N_2 concentrations at the reactor outlet as a function of reactor temperature during the heating after NH_3 adsorption in each cycle. NH_3 and N_2 were the only gaseous products detected during the heating process; no other nitrogen oxide compounds were observed. NH_3 was generated over a temperature range of 50 to 300 °C, indicating that the adsorbed NH_3 molecules were desorbed in their molecular forms in this temperature range (Figure 4b), while N_2 was generated from 150 to 400 °C as a result of NH_3 oxidation on the Fe-oxide/Al_2O_3 surface. The generation profiles for NH_3 and N_2 were almost unchanged in all cycles of the thermal treatment process, i.e., the adsorption capacity of Fe-oxide/Al_2O_3 could be recovered via thermal treatment up to 500 °C. In our experiment, the purging step between NH_3 adsorption and thermal treatments could remove not only the remaining NH_3 gas in the reactor but also the weakly adsorbed NH_3 on the catalyst surface. As they could not be separated easily, it is difficult to determine the exact amount of NH_3 adsorbed on the sample at the beginning of the heating process, limiting our ability to estimate the selectivity of NH_3 or N_2 from the adsorbed NH_3. It is possible that some of adsorbed NH_3 was not desorbed from the surface but remained in oxidized form after thermal oxidation. This suggests that they had either had low surface coverage, which did not affect the total adsorption capacity of the catalyst, or they accumulated on the surface sites irrespective of NH_3 adsorption. Despite the strong recovery of NH_3 adsorption capacity of Fe-oxide/Al_2O_3, molecular desorption of NH_3 during thermal treatment still poses a challenge as it corresponds to secondary emissions of the original pollutant (NH_3) to the atmosphere.

3.5. Dual Catalytic Filters of Fe-Oxide/Al_2O_3 for Energy-Efficient and Clean NH_3 Oxidation. A system with dual catalytic filters was designed to minimize NH_3 emissions to the atmosphere during thermal treatment after NH_3 adsorption (Figure 5). An additional reactor (reactor 2 in Figure 5) containing Fe-oxide/Al_2O_3, the temperature of which could be controlled independently, was installed at the outlet of the existing catalytic reactor (reactor 1 in Figure 5). Our intention was that only the Fe-oxide/Al_2O_3 in reactor 1 was used for NH_3 adsorption at RT, while reactor 2 oxidizes NH_3, emitted from the thermal treatment process of reactor 1, into N_2. When the surface of the catalyst in reactor 1 was about to be saturated with NH_3 at RT, the temperature of reactor 2 was rapidly increased, and when the temperature of reactor 1 was increased gradually, NH_3 molecules desorbed from the

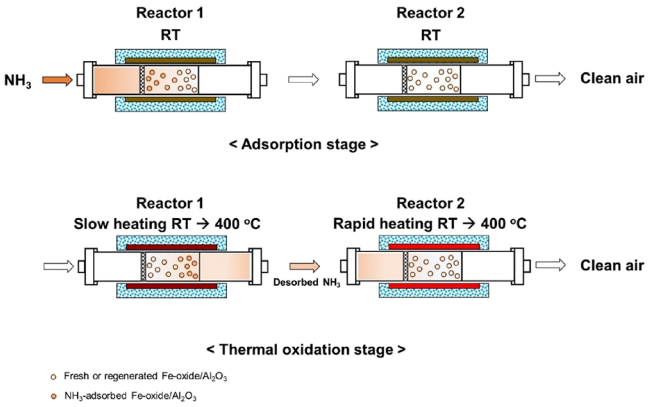

Figure 5. Schematic illustration of dual catalytic filters system for NH_3 decomposition.

catalyst surface of the reactor 1 passed through the sufficiently hot reactor 2 to be converted into N_2. Using this process, not only the emission of NH_3 to the atmosphere but also the energy consumed by the operation of the device for catalytic conversion of NH_3 to N_2 can be reduced.

Figure 6a–c shows the experimental results from the dual catalytic filters, experimental details of which are provided in the experimental section. For comparison, experimental results from the single catalytic filter with same total catalyst amount (Figure 4) are displayed together in Figure 6. Because 2 g of catalyst was placed in each reactor in the system of dual catalytic filters, which is the half amount used in a single reactor, it took about half the time to reach NH_3 adsorption saturation (50 min) with the dual system compared to the single reactor. In the subsequent thermal treatment process, NH_3 was desorbed from 60 to 300 °C in the single reactor. However, in the dual reactors, in which the temperature of reactor 2 was maintained at 400 °C during the thermal treatment process of reactor 1, NH_3 was not detected at any temperature (Figure 6b), indicating that NH_3 desorbed from the catalyst in reactor 1 was totally removed upon passing to reactor 2. Although there was some NH_3 slippage when 2% of NH_3 flowed to catalyst at 400 °C (Figure 2), the concentration of NH_3 desorbed from catalyst in reactor 1 was much lower, so 400 °C was sufficient for reactor 2 to totally remove NH_3.

Using the single reactor, N_2 generation started from approximately 150 °C, whereas it started at 60 °C (temperature of reactor 1) using the dual reactors, which is similar to the NH_3 desorption temperature in the single reactor. In addition, the shape of the N_2 concentration-change profile with the dual reactors was similar to that of NH_3 with the single reactor. Considering that the half amount of NH_3 was adsorbed in the system of dual filters as compared to the single reactor system, it can be stoichiometrically estimated that almost all the desorbed NH_3 in this temperature window was converted into N_2. In the repeated adsorption and thermal oxidation experiment, NH_3 was effectively converted to N_2 without a decrease in catalytic conversion performance. Using the dual catalytic filters of Fe-oxide/Al_2O_3, NH_3 can be efficiently decomposed to N_2 without slippage or oxidation to other gaseous compounds.

4. CONCLUSIONS

Catalytically active Fe-oxide nanoparticles (<2 nm) were deposited on commercial porous Al_2O_3 beads using tr-CVD

https://doi.org/10.1021/acsomega.3c01380
ACS Omega 2023, 8, 18064−18073

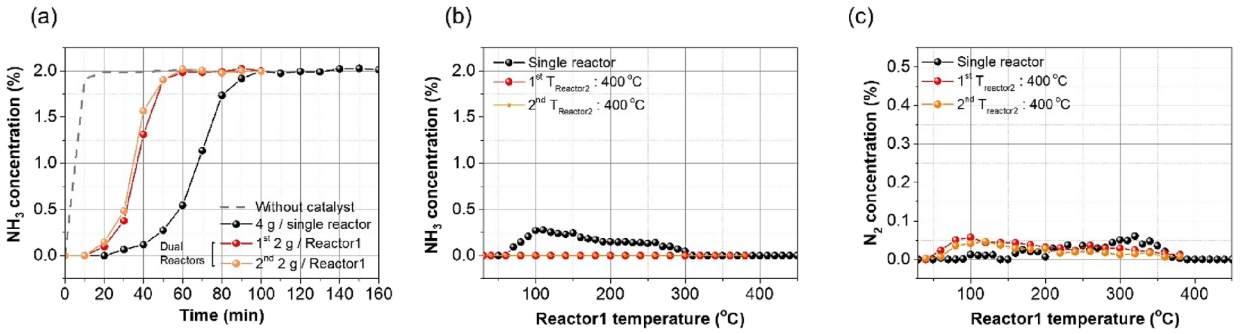

Figure 6. Experimental results obtained from the dual catalytic filters system. (a) Change of NH_3 concentration measured at reactor 1 outlet as a function of NH_3 flow time at RT in the presence of Fe-oxide/Al_2O_3. The gray line represents the change of NH_3 concentration without the catalyst. Change of (b) NH_3 and (c) N_2 concentration measured at the reactor 2 outlet with respect to reactor 1 temperature during the thermal treatment process of NH_3 adsorbed in the catalyst of reactor 1 at RT. The adsorption and thermal treatment using the dual catalytic filters was repeated twice without the replacement of catalyst, and the result of the repeated experiment is included. The results obtained from the single reactor were also included in each figure for comparison. Reaction conditions: 2 g catalyst in reactors 1 and 2, 50 mL/min He balanced gas mixture containing 2% NH_3 and 6% O_2 for NH_3 adsorption, and 49 mL/min ~6% O_2 balanced with He for the thermal treatment of catalyst in reactor 1. The temperature of reactor 2 was set 400 °C during the thermal treatment.

and subsequent annealing, resulting in high dispersion of thermally stable Fe-oxide species throughout the entire porous substrate. Based on XPS, Raman, and NEXAFS analyses, the Fe-oxide nanoparticles appeared to exist in a mixture of 2+ and 3+ oxidation states. The Fe-oxide/Al_2O_3 was able to oxidize NH_3 to N_2 with no harmful gas emissions, including NH_3 and NO_x, at temperatures above 400 °C. Combined analysis of in situ DRIFTS and NAP-NEXAFS suggests a Mars−van Krevelen-type surface NH_3 oxidation mechanism for Fe-oxide/Al_2O_3; the lattice oxygen of Fe-oxide was used to oxidize adsorbed NH_3 to $-NH_2$, which dimerized into N_2H_4 intermediate species and then desorbed as N_2. NH_3 was emitted from the surface between RT and 300 °C during thermal treatment of the Fe-oxide/Al_2O_3 surface precovered with NH_3 at RT. A system with dual catalytic filters of Fe-oxide/Al_2O_3—two interconnected catalytic reactors with independent temperature control—was designed to fully oxidize this desorbed NH_3 to N_2. By heating the rear side reactor to approximately 400 °C prior to thermal treatment of an NH_3-covered surface in the front side of the reactor, the desorbed NH_3 can be oxidized to N_2 via passing the rear-side catalysts. Using this approach, NH_3 can be removed without emissions to the atmosphere with efficient energy consumption.

■ ASSOCIATED CONTENT

Supporting Information

The Supporting Information is available free of charge at https://pubs.acs.org/doi/10.1021/acsomega.3c01380.

Experimental setup and progress of tr-CVD; experimental setup for NH_3 oxidation experiments; XRD patterns of Fe-oxide/Al_2O_3 and bare Al_2O_3; Raman spectrum of Fe-oxide/Al_2O_3 using bare Al_2O_3 spectrum as background; extended NH_3 oxidation activity tests at 450 °C; detailed in situ DRIFTS spectra; Fe L edge spectra under various atmospheric conditions with the deconvoluted peaks; fitting parameters used for the deconvolution; and IR spectra of as-prepared and hydrazine-exposed Fe-oxide/Al_2O_3 (PDF)

■ AUTHOR INFORMATION

Corresponding Author

Young Dok Kim − *Department of Chemistry, Sungkyunkwan University, Suwon, Gyeonggi-do 16419, Republic of Korea;* orcid.org/0000-0003-1138-5455; Email: ydkim91@skku.edu

Authors

Byeong Jun Cha − *Department of Chemistry, Sungkyunkwan University, Suwon, Gyeonggi-do 16419, Republic of Korea; Center of Scientific Instrumentation, Korea Basic Science Institute, Ochang 28119, Republic of Korea*

Ji Yoon Choi − *Department of Chemistry, Sungkyunkwan University, Suwon, Gyeonggi-do 16419, Republic of Korea*

Soo Hyun Kim − *Department of Chemistry, Sungkyunkwan University, Suwon, Gyeonggi-do 16419, Republic of Korea*

Shufang Zhao − *Department of Chemistry, Sungkyunkwan University, Suwon, Gyeonggi-do 16419, Republic of Korea*

Sher Ali Khan − *Department of Chemistry, Sungkyunkwan University, Suwon, Gyeonggi-do 16419, Republic of Korea*

Beomgyun Jeong − *Center for Materials Analysis, Korea Basic Science Institute, Daejeon 34133, Republic of Korea;* orcid.org/0000-0003-3890-1464

Complete contact information is available at: https://pubs.acs.org/10.1021/acsomega.3c01380

Author Contributions

B.J.C. did the conceptualization, investigation, methodology, and writing of the original draft. J.Y.C. and S.H.K. did the methodology and analysis. S.Z. and S.A.K. did the experimentation. B.J. did the methodology, analysis, supervision, and reviewing. Y.D.K. did the project administration, supervision, reviewing, and editing.

Notes

The authors declare no competing financial interest.

■ ACKNOWLEDGMENTS

This work was supported by National Research Foundation of Korea (NRF) grants funded by the Korean government (MSIT) (nos. 2021R1F1A1046312, 2022R1A4A1019296), and research grants from Korea Basic Science Institute

(D300100, C330140, and C330110). The APXPS experiment at PLS-II(BL 8A2) was supported by MSIT and POSTECH.

REFERENCES

(1) Chai, W. S.; Bao, Y.; Jin, P.; Tang, G.; Zhou, L. A Review on Ammonia, Ammonia-Hydrogen and Ammonia-Methane Fuels. *Renew. Sust. Energ. Rev.* **2021**, *147*, No. 111254.
(2) Chmielarz, L.; Jabłońska, M. Advances in Selective Catalytic Oxidation of Ammonia to Dinitrogen: A Review. *RSC Adv.* **2015**, *5*, 43408−43431.
(3) Kobayashi, H.; Hayakawa, A.; Somarathne, K. D.; Kunkuma, A.; Okafor, E. C. Science and Technology of Ammonia Combustion. *Proc. Combust. Inst.* **2019**, *37*, 109−133.
(4) Liu, Y.; Ngo, H. H.; Guo, W.; Peng, L.; Wang, D.; Ni, B. The Roles of Free Ammonia (FA) in Biological Wastewater Treatment Processes: A Review. *Environ. Int.* **2019**, *123*, 10−19.
(5) Valera-Medina, A.; Amer-Hatem, F.; Azad, A. K.; Dedoussi, I. C.; de Joannon, M.; Fernandes, R. X.; Glarborg, P.; Hashemi, H.; He, X.; Mashruk, S.; McGowan, J.; Mounaim-Rouselle, C.; Ortiz-Prado, A.; Ortiz-Valera, A.; Rossetti, I.; Shu, B.; Yehia, M.; Xiao, H.; Costa, M. Review on Ammonia as a Potential Fuel: From Synthesis to Economics. *Energy Fuels* **2021**, *35*, 6964−7029.
(6) Wyer, K. E.; Kelleghan, D. B.; Blanes-Vidal, V.; Schauberger, G.; Curran, T. P. Ammonia Emissions from Agriculture and Their Contribution to Fine Particulate Matter: A Review of Implications for Human Health. *J. Environ. Manage.* **2022**, *323*, No. 116285.
(7) Sommer, S. G.; Hutchings, N. J. Ammonia Emission from Field Applied Manure and Its Reduction—Invited Paper. *Eur. J. Agron.* **2001**, *15*, 1−15.
(8) Maurer, D. L.; Koziel, J. A. On-Farm Pilot-Scale Testing of Black Ultraviolet Light and Photocatalytic Coating for Mitigation of Odor, Odorous VOCs, and Greenhouse Gases. *Chemosphere* **2019**, *221*, 778−784.
(9) McCrory, D. F.; Hobbs, P. J. Additives to Reduce Ammonia and Odor Emissions from Livestock Wastes: A Review. *J. Environ. Qual.* **2001**, *30*, 345−355.
(10) Gonçalves, M.; Sánchez-García, L.; Oliveira Jardim, E.; Silvestre Albero, J.; Rodríguez Reinoso, F. Ammonia Removal Using Activated Carbons: Effect of the Surface Chemistry in Dry and Moist Conditions. *Environ. Sci. Technol.* **2011**, *45*, 10605−10610.
(11) Byeon, S.-H.; Lee, B.-K.; Raj Mohan, B. Removal of Ammonia and Particulate Matter Using a Modified Turbulent Wet Scrubbing System. *Sep. Purif. Technol.* **2012**, *98*, 221−229.
(12) Bandosz, T. J.; Petit, C. On the Reactive Adsorption of Ammonia on Activated Carbons Modified by Impregnation with Inorganic Compounds. *J. Colloid Interface Sci.* **2009**, *338*, 329−345.
(13) Schüth, F.; Palkovits, R.; Schlögl, R.; Su, D. S. Ammonia as A Possible Element in An Energy Infrastructure: Catalysts for Ammonia Decomposition. *Energy Environ. Sci.* **2012**, *5*, 6278−6289.
(14) Lee, S.-H.; Li, C.; Heber, A. J.; Ni, J.; Huang, H. Biofiltration of A Mixture of Ethylene, Ammonia, N-Butanol, and Acetone Gases. *Bioresour. Technol.* **2013**, *127*, 366−377.
(15) Monnery, W. D.; Hawboldt, K. A.; Pollock, A. E.; Svrcek, W. Y. Ammonia Pyrolysis and Oxidation in the Claus Furnace. *Ind. Eng. Chem. Res.* **2001**, *40*, 144−151.
(16) Lan, T.; Zhao, Y.; Deng, J.; Zhang, J.; Shi, L.; Zhang, D. Selective Catalytic Oxidation of NH_3 over Noble Metal-Based Catalysts: State of the Art and Future Prospects. *Catal. Sci. Technol.* **2020**, *10*, 5792−5810.
(17) Long, R. Q.; Yang, R. T. Selective Catalytic Oxidation of Ammonia to Nitrogen over Fe_2O_3−TiO_2 Prepared with A Sol−Gel Method. *J. Catal.* **2002**, *207*, 158−165.
(18) Jabłońska, M. Progress on Selective Catalytic Ammonia Oxidation (NH_3-SCO) over Cu−Containing Zeolite-Based Catalysts. *ChemCatChem* **2020**, *12*, 4490−4500.
(19) Hinokuma, S.; Sato, K. Ammonia Combustion Catalysts. *Chem. Lett.* **2021**, *50*, 752−759.
(20) Jeong, J. H.; Kim, S. Y.; Kim, J.; Cha, B. J.; Han, S. W.; Park, C. H.; Woo, T. G.; Kim, C. S.; Kim, Y. D. Adsorption and Oxidative Desorption of Acetaldehyde over Mesoporous $Fe_xO_yH_z/Al_2O_3$. *ACS Omega* **2019**, *4*, 5382−5391.
(21) Yang, C.; Miao, G.; Pi, Y.; Xia, Q.; Wu, J.; Li, Z.; Xiao, J. Abatement of Various Types of VOCs by Adsorption/Catalytic Oxidation: A Review. *Chem. Eng. J.* **2019**, *370*, 1128−1153.
(22) Cha, B. J.; Choi, J. Y.; Kim, S. Y.; Kim, Y. D. Adsorbent/Catalyst Bi-Functional Fe-ZSM-5 Prepared by a Simple CVD Process for Exhaust Gas Treatment. *Appl. Surf. Sci.* **2022**, *574*, No. 151565.
(23) Cha, B. J.; Choi, J. Y.; Ji, Y.; Zhao, S.; Kim, S. Y.; Kim, S. H.; Kim, Y. D. Fe-oxide/Al_2O_3 for the Enhanced Activity of H_2S Decomposition Under Realistic Conditions: Mechanistic Studies by In-Situ DRIFTS and XPS. *Chem. Eng. J.* **2022**, *443*, No. 136459.
(24) Cha, B. J.; Ji, Y.; Choi, C. M.; Jung, D.; Hwang, C.-C.; Chae, H. C.; Choi, M. C.; Seo, H. O.; Kim, Y. D. Role of Fe−C−Al Sites for Low-Temperature CO Oxidation (∼50 °C) over the Fe-Oxide Nanoparticles Supported by Al_2O_3. *J. Phys. Chem. C* **2022**, *126*, 13686−13697.
(25) Cha, B. J.; Kim, I. H.; Park, C. H.; Choi, C. M.; Sung, J. Y.; Choi, M. C.; Kim, Y. D. Reduction of NO by CO Catalyzed by Fe-oxide/Al_2O_3: Strong Catalyst-Support Interaction for Enhanced Catalytic Activity. *Appl. Surf. Sci.* **2020**, *509*, No. 145300.
(26) Kim, M. S.; Lee, D. W.; Chung, S. H.; Hong, Y. K.; Lee, S. H.; Oh, S. H.; Cho, I. H.; Lee, K. Y. Oxidation of Ammonia to Nitrogen over Pt/Fe/ZSM5 Catalyst: Influence of Catalyst Support on the Low Temperature Activity. *J. Hazard. Mater.* **2012**, *237-238*, 153−160.
(27) Zhang, Q.; Wang, H.; Ning, P.; Song, Z.; Liu, X.; Duan, Y. In Situ DRIFTS Studies on CuO-Fe_2O_3 Catalysts for Low Temperature Selective Catalytic Oxidation of Ammonia to Nitrogen. *Appl. Surf. Sci.* **2017**, *419*, 733−743.
(28) Kim, I. H.; Seo, H. O.; Park, E. J.; Han, S. W.; Kim, Y. D. Low Temperature CO Oxidation over Iron Oxide Nanoparticles Decorating Internal Structures of a Mesoporous Alumina. *Sci. Rep.* **2017**, *7*, 40497.
(29) Saqlain, S.; Cha, B. J.; Kim, S. Y.; Ahn, T. K.; Park, C.; Oh, J.-M.; Jeong, E. C.; Seo, H. O.; Kim, Y. D. Visible Light-Responsive Fe-Loaded TiO_2 Photocatalysts for Total Oxidation of Acetaldehyde: Fundamental Studies Towards Large-Scale Production and Applications. *Appl. Surf. Sci.* **2020**, *505*, No. 144160.
(30) Hong, Y.; Cha, B. J.; Kim, Y. D.; Seo, H. O. Mesoporous SiO_2 Particles Combined with Fe Oxide Nanoparticles as a Regenerative Methylene Blue Adsorbent. *ACS Omega* **2019**, *4*, 9745−9755.
(31) Kruk, M.; Jaroniec, M. Gas Adsorption Characterization of Ordered Organic−Inorganic Nanocomposite Materials. *Chem. Mater.* **2001**, *13*, 3169−3183.
(32) Gupta, R. P.; Sen, S. K. Calculation of Multiplet Structure of Core p-Vacancy Levels. *Phys. Rev. B* **1974**, *10*, 71−77.
(33) Gupta, R. P.; Sen, S. K. Calculation of Multiplet Structure of Core p-Vacancy Levels. *Phys. Rev. B* **1975**, *12*, 15−19.
(34) Grosvenor, A. P.; Kobe, B. A.; Biesinger, M. C.; McIntyre, N. S. Investigation of Multiplet Splitting of Fe 2p XPS Spectra and Bonding in Iron Compounds. *Surf. Interface Anal.* **2004**, *36*, 1564−1574.
(35) Ma, L.; Li, Z.; Zhao, H.; Zhang, T.; Yan, N.; Li, J. Understanding the Water Effect for Selective Catalytic Reduction of NO_x with NH_3 over Cu-SSZ-13 Catalysts. *ACS EST Eng.* **2022**, *2*, 1684−1696.
(36) Li, Y.; Armor, J. N. Selective NH_3 Oxidation to N_2 in A Wet Stream. *Appl. Catal., B* **1997**, *13*, 131−139.
(37) Dann, E. K.; Gibson, E. K.; Blackmore, R. H.; Catlow, C. R. A.; Collier, P.; Chutia, A.; Erden, T. E.; Hardacre, C.; Kroner, A.; Nachtegaal, M.; Raj, A.; Rogers, S. M.; Taylor, S. F. R.; Thompson, P.; Tierney, G. F.; Zeinalipour-Yazdi, C. D.; Goguet, A.; Wells, P. P. Structural Selectivity of Supported Pd Nanoparticles for Catalytic NH_3 Oxidation Resolved Using Combined Operando Spectroscopy. *Nat. Catal.* **2019**, *2*, 157−163.
(38) Zhang, L.; He, H. Mechanism of Selective Catalytic Oxidation of Ammonia to Nitrogen over Ag/Al_2O_3. *J. Catal.* **2009**, *268*, 18−25.
(39) Ramis, G.; Angeles Larrubia, M. An FT-IR Study of the Adsorption and Oxidation of N-Containing Compounds over Fe_2O_3/Al_2O_3 SCR Catalysts. *J. Mol. Catal. A: Chem.* **2004**, *215*, 161−167.

https://doi.org/10.1021/acsomega.3c01380
ACS Omega 2023, 8, 18064−18073

(40) Ramis, G.; Yi, L.; Busca, G. Ammonia Activation over Catalysts for the Selective Catalytic Reduction of NO_x and the Selective Catalytic Oxidation of NH_3. *An FT-IR Study. Catal. Today* **1996**, *28*, 373−380.
(41) Goebbert, D. J.; Garand, E.; Wende, T.; Bergmann, R.; Meijer, G.; Asmis, K. R.; Neumark, D. M. Infrared Spectroscopy of the Microhydrated Nitrate Ions $NO_3^-(H_2O)_{1-6}$. *J. Phys. Chem. A* **2009**, *113*, 7584−7592.
(42) Amores, J. G.; Escribano, V. S.; Ramis, G.; Busca, G. An FT-IR Study of Ammonia Adsorption and Oxidation over Anatase-Supported Metal Oxides. *Appl. Catal.* **1997**, *13*, 45−58.
(43) Sil'chenkova, O. N.; Korchak, V. N.; Matyshak, V. A. The Mechanism of Low-Temperature Ammonia Oxidation on Metal Oxides According to the Data of Spectrokinetic Measurements. *Kinet. Catal.* **2002**, *43*, 363−371.
(44) Pérez-Ramírez, J.; Kondratenko, E. V. Mechanism of Ammonia Oxidation over Oxides Studied by Temporal Analysis of Products. *J. Catal.* **2007**, *250*, 240−246.
(45) Lin, M.; An, B.; Niimi, N.; Jikihara, Y.; Nakayama, T.; Honma, T.; Takei, T.; Shishido, T.; Ishida, T.; Haruta, M.; Murayama, T. Role of the Acid Site for Selective Catalytic Oxidation of NH_3 over Au/Nb_2O_5. *ACS Catal.* **2019**, *9*, 1753−1756.
(46) Miedema, P. S.; de Groot, F. M. F. The Iron L Edges: Fe 2p X-ray Absorption and Electron Energy Loss Spectroscopy. *J. Electron Spectrosc. Relat. Phenom.* **2013**, *187*, 32−48.
(47) Hidalgo, T.; Giménez-Marqués, M.; Bellido, E.; Avila, J.; Asensio, M. C.; Salles, F.; Lozano, M. V.; Guillevic, M.; Simón-Vázquez, R.; González-Fernández, A.; Serre, C.; Alonso, M. J.; Horcajada, P. Chitosan-Coated Mesoporous MIL-100(Fe) Nanoparticles as Improved Bio-Compatible Oral Nanocarriers. *Sci. Rep.* **2017**, *7*, 43099.
(48) Mars, P.; van Krevelen, D. W. Oxidations Carried Out by Means of Vanadium Oxide Catalysts. *Chem. Eng. Sci.* **1954**, *3*, 41−59.
(49) Ross, J. R. H. The Kinetics and Mechanisms of Catalytic Reactions. In *Contemporary Catalysis*; Ross, J. R. H., Ed.; Elsevier: Amsterdam, 2019; pp. 161−186, DOI: 10.1016/B978-0-444-63474-0.00007-2
(50) Ruan, C.; Wang, X.; Wang, C.; Zheng, L.; Li, L.; Lin, J.; Liu, X.; Li, F.; Wang, X. Selective Catalytic Oxidation of Ammonia to Nitric Oxide via Chemical Looping. *Nat. Commun.* **2022**, *13*, 718.

https://doi.org/10.1021/acsomega.3c01380
ACS Omega 2023, 8, 18064−18073